Electrochimica Acta 537 (2025) 146849

Contents lists available at ScienceDirect

Electrochimica Acta

journal homepage: www.journals.elsevier.com/electrochimica-acta

Alumina and hafnia thin films deposited by atomic layer deposition at different temperatures on biomedical stainless steel and titanium

Ivan Spajić [a,b], Sandra Drev [c], Urška Trstenjak [d], Ingrid Milošev [a,b,*]

[a] Department of Physical and Organic Chemistry, Jožef Stefan Institute, Jamova cesta 39, 1000 Ljubljana, Slovenia
[b] Jožef Stefan International Postgraduate School, Jamova cesta 39, 1000 Ljubljana, Slovenia
[c] Center for Electron Microscopy and Microanalysis, Jožef Stefan Institute, Jamova cesta 39, 1000 Ljubljana, Slovenia
[d] Department of Advanced Materials, Jožef Stefan Institute, Jamova cesta 39, 1000 Ljubljana, Slovenia

ARTICLE INFO

Keywords:
Atomic layer deposition ALD
Alumina
Hafnia
Stainless steel
Titanium

ABSTRACT

Alumina and hafnia films produced by the atomic layer deposition were applied to commercially pure Ti and stainless steel 316L specimens for protection under simulated human body conditions. The ALD films were deposited at 180 °C and 260 °C to determine how the deposition temperature affect the films' protective properties. Surface analysis of the ALD films included scanning electron microscopy, transmission electron microscopy, X-ray diffraction, and X-ray photoelectron spectroscopy. The barrier properties were tested electrochemically using potentiodynamic polarisation and electrochemical impedance spectroscopy (EIS) techniques in a simulated body solution at 37 °C. Alumina thin films showed substantial barrier properties, but after 30 days of immersion, the alumina dissolved regardless of the deposition temperature. EIS tests themselves promoted the dissolution of alumina. In contrast, the barrier properties of hafnia depended significantly on deposition temperature. Hafnia deposited at 180 °C exhibited substantial protective properties and remarkable stability over an extended immersion period. However, when deposited at 260 °C hafnia films showed strong protection at the outset, but after a few days of immersion, they lost their protective ability due to porosity. The key factors affecting the barrier properties of ALD hafnia films were the proportion of the crystalline phase and how crystallites formed.

1. Introduction

Titanium-based alloys, stainless steel and Co-Cr-based alloys are the most used metallic materials for medical purposes, primarily as implant devices [1]. The choice for these materials is based on their mechanical properties and chemical stability, i.e. resistance to corrosion in the human body fluids, which ultimately reflects on the biocompatibility of the material [2,3]. However, due to different chemical and mechanical properties, these materials are used for different purposes [1,3]. For example, commercially pure Ti (cp-Ti) is characterised by the best corrosion resistance thanks to the naturally formed thin passive titania (TiO_2) film that effectively protects it in a wide range of potentials and pH values [4–6]. However, it is susceptible to fretting corrosion, i.e. corrosion supported by mechanical wear of the material [7,8]. Because of that, cp-Ti is used for implant parts not exposed to mechanical loads, such as pacemakers, artificial heart valves, and dental and maxillofacial implants [8]. On the other hand, medical stainless steel 316L (SS316L) has better mechanical properties, i.e. strength and wear resistance, than cp-Ti [9], but it is susceptible to pitting corrosion, which can cause severe consequences due to the release of toxic metal ions (Cr and Ni) into the human body [3,6,10]. Therefore, SS316L is mainly used for temporary implant components (like screws, plates, nails, etc.) [2].

Due to the drawbacks mentioned above, various methods were used to improve surface properties, either mechanical features or corrosion resistance [11]. For example, implantation of the N ions [12,13] and surface plasma treatment [11] were often used. Also, different types of physical vapour deposition (PVD) [14,15] and chemical vapour deposition (CVD) [16] techniques are being investigated. One such technique, a subtype of the CVD technique, is atomic layer deposition (ALD) [17], which enables the formation of nanometric thin films with high thickness uniformity and conformity on very complex nano-shaped surfaces or even inside nanoporous materials [18,19]. Another advantage of the ALD technique is the possibility of forming defect- and impurity-free films based on a pure gas-to-solid chemical reaction [20].

* Corresponding author.
E-mail address: ingrid.milosev@ijs.si (I. Milošev).

https://doi.org/10.1016/j.electacta.2025.146849
Received 5 May 2025; Received in revised form 1 July 2025; Accepted 3 July 2025
Available online 4 July 2025

Thanks to the applications in numerous fields of science and technology, ALD processes have been developed targeting different materials [21]. In the medical field, the focus has remained mainly on a few materials suitable for these applications. These are films of alumina (Al_2O_3) [22–25], zirconia (ZrO_2) [26–28], titania (TiO_2) [27,29,30], and hydroxyapatite (HA) [31] as bioactive material. However, despite the high uniformity and the possibility of producing defect-free thin films, ALD films have some drawbacks that need further investigation to establish their application in medicine. Namely, if alumina is deposited below 600 °C, it forms an amorphous film, which acts as a good barrier in terms of corrosion protection [32]. However, under certain conditions, an amorphous film shows instability in water solutions [33,34]. On the other hand, some metal oxides, such as titania [20,35], zirconia [36] and hafnia (HfO_2) [36,37] quickly form a crystalline phase already at lower temperatures, so that corrosive species from the surrounding fluid can reach the boundaries of the crystal grains [32,35]. Due to the cost-effectiveness and duration of the ALD processes, nanometer-thick films are usually deposited up to 100 nm. Such films will be damaged if mechanically loaded under wear conditions, representing another general disadvantage of ALD films. Therefore, applying ALD thin films in medicine is limited to parts of orthopaedic implants that are not subjected to contact wear, e.g. dental, cardiovascular and cochlear implants [38]. ALD is also used for specific applications in biotechnology, such as biosensors and diagnostics, modification of nanoporous materials, biotemplating, etc. [39].

The deposition of alumina has hitherto been the most studied ALD process [40]. Thanks to the long-lasting, well-established use of alumina in the bulk form in medicine [41,42], several studies aimed to modify different substrates for medical applications with alumina ALD films [22–25]. Of these, only one study focused on the protective properties of ALD alumina on a metal substrate (SS316L), proving to be a promising solution for the corrosion susceptibility of SS316L under human body conditions [22]. Generally, in all studies [22–25], ALD alumina was presented as a potentially usable material for implantation devices. However, some studies not related to medical applications have warned about the possible instability and solubility of ALD alumina in different media, including aqueous solutions [33,34].

Another metal oxide obtained by the ALD method, which has been widely researched in electronics as a dielectric material, is hafnia [43,44]. For medical purposes, ALD hafnia has been investigated only by our group so far. The exceptional stability of hafnia in simulated body conditions and good barrier properties during 40 days of immersion were established when deposited as a relatively thick film of 150 nm and on the chemo-mechanically polished cp-Ti [45]. In addition, the biocompatibility of hafnia films obtained by anodic oxidation was investigated, but without considering the barrier properties [46]. Interestingly, some studies dealt with pure metal Hf as an alternative metal for implantation as it is chemically very similar to Ti and analogously passivated with a protective layer of hafnia, although much heavier [47]. Hf, when implanted in mammal tissue, have the same response as Ti and, in general, the potential usability for the production of implants [47,48]. Hafnia film, produced by ALD, has been scarcely investigated as protection in the field of corrosion, although it is known to have good insulating properties due to its good dielectric properties [49]. Thus, Daubert et al. reported that among several different metal oxides produced by ALD (Al_2O_3, TiO_2, ZnO, HfO_2, and ZrO_2), hafnia exhibits the best coating quality after extended exposure in aqueous NaCl solution [35]. In addition, in a favourable temperature range, from 100 °C to 350 °C, ALD hafnia film shows an increase in crystallinity, which allows controlling the protective properties as well [37,50].

This study continues and complements the previous studies; in the first, we focused on the protective properties of alumina and hafnia ALD films of 160 and 150 nm in thickness [45], and in the second, on 20 and 60 nm thick films of alumina and alumina in combination with hafnia [51]. Also, our recently published study, where we focused exclusively on biological research, i.e. their biocompatibility and antibacterial properties, has shown that these materials in the form of thin films are worthy of further research [52]. This study deals with the effect of the deposition temperature on the protective properties of alumina and hafnia ALD films over a longer period of exposure to simulated conditions of the human body. ALD films of 80 and 60 nm in thickness were deposited at 180 °C and 260 °C and tested immediately after deposition (mark "as-deposited") and during long-term exposure in simulated human body conditions. As substrates, polished cp-Ti and SS316L were used. The protective properties of alumina and hafnia films were tested using potentiodynamic polarisation (PDP) technique and electrochemical impedance spectroscopy (EIS) to evaluate stability during long-term exposure. For additional characterisation of the ALD films, scanning electron microscopy (SEM) for investigation of the morphology, grazing incidence X-ray diffraction (GI-XRD) to determine the crystallinity of the films and focused ion beam (FIB) for inspection of structure and thickness at the cross-section site, were performed. Transmission electron microscopy (TEM) analysis was applied exclusively for a detailed inspection of the hafnia films regarding the formation of aggregates. X-ray photoelectron spectroscopy (XPS) surface analysis and depth profiling were employed for the elemental and speciation analysis of specimens subject to electrochemical analysis.

2. Experimental part

2.1. Substrate materials

Cp-Ti and SS316L specimens in the shape of a disc of 2.0 mm in thickness and 15 mm in diameter, supplied by GoodFellow Cambridge Ltd., were used as substrate materials. The cp-Ti was grade 2, with a high purity of 99.6 %, and SS316L with the composition of the main alloying elements as follows: 18 wt. % Cr, 10 wt. % Ni and 3 wt. % Mo, rest Fe, as reported by the supplier.

Both materials, cp-Ti and SS316L, were ground and then polished until a mirror-like surface appearance (LaboPol-5, Struers). Grinding was performed gradually with SiC emery papers of 500, 1000 and 2400 grit (Struers, Denmark), followed by chemical-mechanical polishing with silica (SiO_2) suspension (OP-S) with a particle size of 0.25 μm on a suitable material according to Struers' recommendations, and with controlled addition of chemical reagents. For cp-Ti, 30 % H_2O_2 and 25 % NH_4OH (Merck KGaA) were used, while for SS316L, 30 % H_2O_2 and 3.5 % HCl (Merck KGaA). Afterwards, the specimens were successively rinsed with Milli-Q water and cleaned in 99.6 % ethanol (Merck KGaA) using an Elmasonic series P ultrasonic bath (Elma Schmidbauer GmbH) for 15 min and then dried with high-pressured nitrogen gas. Such prepared specimens were stored overnight (about 16 h) in a vacuum desiccator filled with commercial hygroscopic silica gel to ensure uniform surface conditions before ALD depositions or electrochemical tests.

2.2. Atomic layer deposition procedures

Thin films of alumina (Al_2O_3) and hafnia (HfO_2) were deposited using a TFS 200 system from Beneq Oy. Alumina was deposited using trimethylaluminium ($Al(CH_3)_3$ or TMA, 99.99 % PURATREM, STREM Chemicals Inc.) as the first precursor. Hafnia was deposited using tetrakis(ethylmethylamido)hafnium(IV) ($Hf[N(CH_3)(C_2H_5)]_4$ or TEMAH, 99.99 % PURATREM, STREM Chemicals Inc.) as the first precursor. Milli-Q water (resistivity 18 MΩ cm^2 at 25 °C, Billerica, MA) served as the second precursor for both types of films. For alumina, the ALD cycle consisted of a 0.35 s TMA dose, a 2 s N_2 purge, a 0.3 s water dose, and a 2 s N_2 purge, with an assumed growth rate per cycle (GPC) of ca. 1 Å/cycle, as reported previously with similar conditions [53–55]. For hafnia, the ALD cycle consisted of a 0.5 s TEMAH dose, a 2 s N_2 purge, a 0.2 s water dose, and a 2 s N_2 purge, with an assumed GPC of 0.95 Å/cycle. These parameters were optimised in previous experiments (unpublished) and are partially based on earlier reports [36,55,56]. The target thicknesses of the alumina and hafnia ALD films were 60 nm, and

accordingly, 600 cycles for alumina and 630 cycles for hafnia films were performed. Both described ALD procedures were performed at 180 °C and 260 °C. The notation of the specimens is shown in Table 1.

2.3. Electrochemical measurements

All electrochemical measurements were performed using potentiostats/galvanostats with electrochemical impedance modulus, Autolab PGSTATs 302 N, M204 and 12, controlled by Nova 2.1.4 software, supplied by Metrohm AG. The standard three-electrode system was used with an Ag/AgCl (3 M KCl) electrode (E = 0.192 V vs. SHE) as the reference electrode and a carbon rod as the counter electrode. The specimen, serving as a working electrode, was tightened in a suitable Teflon holder with a 1 cm^2 area exposed to the electrolyte solution. All the potentials in the text are given with respect to the Ag/AgCl electrode. The electrochemical tests were performed in an Autolab 400 mL corrosion cell thermostated at 37 ± 0.1 °C, with the Hanks' solution as the electrolyte, with a pH of 7.4, simulating human body conditions. The composition of the Hanks' simulated physiological solution is given in Table 2. All chemicals used to prepare the electrolyte were of *p.a.* purity and were supplied by Merck and Sigma-Aldrich.

Specimens were subjected to cyclic potentiodynamic polarisation (PDP) and electrochemical impedance spectroscopy (EIS) tests. Before the PDP tests, specimens were allowed to rest and stabilise for a minimum of 1 h at the open circuit potential (OCP). PDP curves were obtained using a scan rate of 1 mV/s, starting at −0.1 V vs. OCP to avoid possible hydrogen adsorption on the metal surface. In the case of cp-Ti specimens, polarisation in the anodic direction was allowed up to 4 V for uncoated and even up to 6 V for ALD-coated specimens. For the SS316L specimens, due to susceptibility to pitting corrosion, the polarisation in the anodic direction continued until the current reached a value of 10^{-3} A/cm^2.

The long-term EIS tests were performed for non-coated and coated specimens using the same procedure. Frequencies ranged from 100 kHz to 1 mHz, and an AC excitation voltage was 10 mV (rms, root-mean-square), with a frequency step of 7 points per decade. The tests were performed after selected immersion times: 1 h, 5 d, 15 d, 20 d, 30 d, 40 d and 50 d, but only representative measurements are shown in this study. Although the EIS technique is considered non-destructive, for comparison, the second group of specimens was immersed in the Hanks' solution for 50 days, but without EIS measurements. Both types of specimens were then analysed by XPS.

2.4. Material and surface characterisation

Morphological features of uncoated and ALD-coated specimens were analysed by scanning electron microscopy (SEM), FEI Helios 650 Nanolab. Specimens have been coated with a several-nanometer-thick layer of carbon to avoid charging. SEM imaging was performed at a beam acceleration voltage of 3 kV to gather information on the topmost surface of the specimens. Cross-section surfaces of ALD-coated specimens were obtained using a focused ion beam (FIB), FEI Helios 650 Nanolab, with Ga^+ ions as an etching beam. Before the analysis, an additional 2.5 μm-thick Pt protective layer was deposited over the selected site. The cross-section was then made by rough etching of ALD films and fine polishing using a lower current. Then, the cross-section images were taken by SEM to check the homogeneity and thickness of the ALD films.

Table 1
Notation of specimens used in the study.

Specimen	Notation	Specimen	Notation
commercially pure Ti	cp-Ti	stainless steel 316L	SS613L
cp-Ti coated with ALD alumina deposited at 180 °C	Ti-AL180	SS coated with ALD alumina deposited at 180 °C	SS-AL180
cp-Ti coated with ALD alumina deposited at 260 °C	Ti-AL260	SS coated with ALD alumina deposited at 260 °C	SS-AL260
cp-Ti coated with ALD hafnia deposited at 180 °C	Ti-HF180	SS coated with ALD hafnia deposited at 180 °C	SS-HF180
cp-Ti coated with ALD hafnia deposited at 260 °C	Ti-HF260	SS coated with ALD hafnia deposited at 260 °C	SS-HF260

Table 2
Chemical composition of the Hanks' simulated physiological solution.

Components	Concentration (g dm^{-3})
NaCl	8.0
KCl	0.40
$NaHCO_3$	0.35
$CaCl_2$	0.14
$MgCl_2 \cdot 6H_2O$	0.10
$MgSO_4 \cdot 7H_2O$	0.06
$Na_2HPO_4 \cdot 2H_2O$	0.06
KH_2HPO_4	0.06
Glucose	1.0

Detailed structural investigations of cp-Ti specimens coated with hafnia films were performed by transmission electron microscopy (TEM), JEOL JEM-2010F, equipped with Oxford Instruments EDS ISIS 300 system. For this purpose, selected specimens were prepared as lamellas using FIB, FEI Helios 650 Nanolab. This was performed by using Ga^+ ions as an etching beam. Final polishing was performed with Ga^+ ions at 1 kV/100 pA for 1 min on each side, enabling the removal of the amorphous residue and gallium artefacts. The final thickness of the lamella was below 50 nm.

For surface analyses and depth profiling after EIS long-term tests and after immersion of 50 days in tested conditions, X-ray photoelectron spectroscopy (XPS), Physical Electronics PHI-TFA, was used. The analysed area was 0.1 mm^2, and the depth analysis was 3–5 nm. As the source of X-rays, an Al-anode with a monochromator with photon emission energy of 1486.6 eV and an analysed area of 400 μm in diameter was used. The depth profile was obtained using a 3 keV Ar^+ ion beam rastering over 3 × 3 mm, with a sputtering rate of 1.5 nm/min for alumina and 1.0 nm/min for hafnia films. Commercial SiO_2 was used as a standard for determining the etching rate. XPS spectra were analysed by Multipack V8.1 C software (Physical Electronics Inc.) and were normalised relative to the position of the C 1 s peak at 284.8 eV. The binding energy positions of the main metal and nonmetal peaks were corrected relative to the position of the C 1 s peak at 284.8 eV.

X-ray diffractometry (XRD), Empyrean Malvern PANalyticalm, in grazing incidence (GI-XRD) mode, was used to estimate the crystallinity of the ALD films. Measurements were performed with Cu Kα1 radiation (λ = 1.5406 Å) at 45 kV and 40 mA. A hybrid monochromator with a 1/16° slit was used on the incident beam side, and a parallel plate collimator with a 0.27° opening was used on the diffracted beam side. The GI angle (ω) was fixed at 1°, and the X-ray patterns were collected in the 2θ range from 20° to 80° with a step size of 0.02°.

3. Results and discussion

3.1. Materials and surface characterisation

The method, supported by the chemical action of the reagents, produces mirror-like surfaces of cp-Ti and SS316L with visible crystal grains under SEM investigation. The smoothness of the surfaces is of the order of 10 nm, as reported in the previous work [45]. Developed preparational procedures ensured the most uniform conditions on both substrates equally and were suitable for subsequent characterisation of the ALD films. SEM characterisation for polished surfaces of cp-Ti and SS316L has been demonstrated in previous articles [45,51].

Fig. 1 shows the surface morphologies of as-deposited ALD films. The morphology of alumina films depends on the substrate, while there are no differences when they were deposited at different temperatures, 180 °C and 260 °C. In Fig. 1**a and b,** examples are given for Ti-AL180 and SS-AL260, and the images for Ti-AL260 and SS-AL180 are shown in the Supplemental information (**Fig. S1a and b**). During the deposition process, aggregates of various sizes formed on both substrates. Most aggregates were sized approximately 1 μm (Fig. 1**a and b**) and may represent weak spots due to possible electrolyte leakage around them. However, in the case of SS316L, a larger portion of smaller aggregates was present over the substrate surface (Fig. 1**b**). These aggregates can be caused in two ways: (1) by non-ideal gas-to-solid ALD reaction [21], and (2) by surface irregularities and defects on the substrate that can trigger accelerated aggregate growth within the continuous film [57]. A non-ideal ALD reaction may result from deposition temperatures that are too low, preventing the precursor from fully reacting, or from excessively high temperatures, which can lead to thermal decomposition of the precursor upon contact with the hot substrate. In both cases, the result can be a localised accumulation of deposited material and unwanted species on random areas of the substrate surface. However, in this study, depositions were carried out using usual ALD parameters, and at temperatures commonly used for the TMA precursor [40,54]. Furthermore, the morphology of the aggregates appears similar at both low and high deposition temperatures—i.e., at 180 °C and 260 °C—but differs significantly between substrates, cp-Ti and SS-316 L. This suggests that the formation of aggregates is primarily influenced by the surface characteristics of each substrate, likely due to grain boundary defects or imperfect surface polishing [51].

Unlike alumina, hafnia films showed different morphologies at different temperatures, regardless of the type of substrate (Fig. 1**c and d**). Examples are given for films deposited on SS316L, whereas images for films deposited on cp-Ti are given in the Supplemental Information (**Fig. S1c and d**). The hafnia film deposited at 180 °C had a uniform surface without large aggregates (Fig. 1**c**), but on the lower scale, it can be seen that it is composed of nanometric grains (**inset in** Fig. 1**c**). However, when deposited at 260 °C, the films were rich in micrometre-sized aggregates (Fig. 1**d**). The latter seems to be the characteristic feature of ALD hafnia film grown at higher temperatures, i.e. at 260 °C. In this case, the nanometric grains form the main part of the film as well, but they are more densely distributed (inset in Fig. 1**d**) than hafnia deposited at 180 °C. A similar morphology of hafnia thin films, i.e., thin films composed of nanometric grains, has been observed in a previous study [58], and this will be discussed in more detail later based on the TEM results. Thus, in the case of hafnia thin film deposition, the type of substrate does not significantly influence the film morphology; however, temperature is a key parameter that determines the surface appearance of the films.

Regarding the thicknesses of the ALD films, the alumina was grown with a slightly higher GPC than expected, giving thicker films (ca. 80 nm), while in the case of the hafnia films, they corresponded to a thickness of about 60 nm with non-uniformity in the case of 260 °C due to the presence of the big aggregates. Related results of FIB cross-sections on the ALD films on both substrates are given in the Supplemental information (**Fig. S2 and S3**).

The presence of a crystal phase may represent a drawback regarding the barrier properties of the ALD films, due to the possibility of electrolyte leakage at the crystal grain boundaries [20,32]. In the case of hafnia, it has been reported that if grown above 200 °C, it tends to form a crystalline phase [37,50]. Considering the appearance of large aggregates at higher temperatures (Fig. 1**d**), it could be assumed that they are related to crystalline grains. This is further investigated using GI-XRD and TEM investigations. GI-XRD measurements were made to determine if there is a difference in crystallinity between ALD films deposited at lower and higher temperatures. As a substrate, cp-Ti was chosen for simplicity. As expected, alumina was amorphous regardless of the deposition temperatures (Fig. 2**a**), considering alumina tends towards

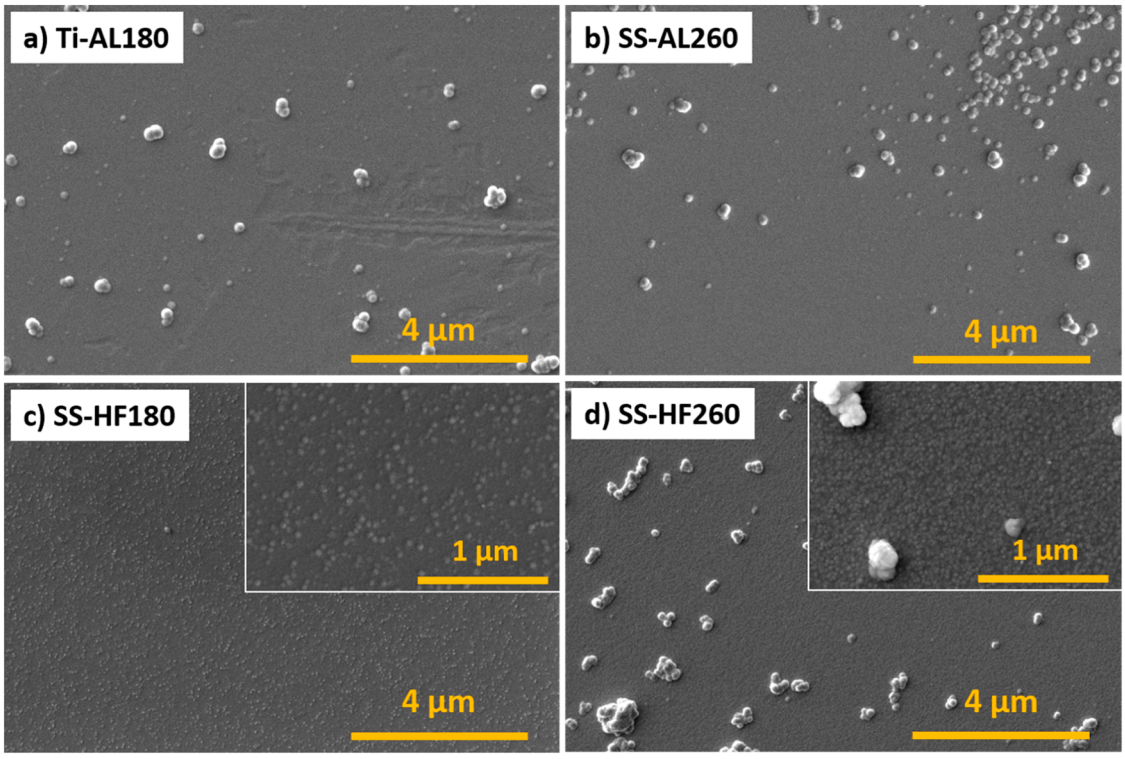

Fig. 1. SEM images of ALD coated cp-Ti and SS316L substrates; **a)** surface morphology of alumina deposited on cp-Ti at 180 °C, **b)** surface morphology of alumina deposited on SS316L at 260 °C, **c)** surface morphology of hafnia deposited at 180 °C on SS316L, **d)** surface morphology of hafnia deposited at 260 °C on SS316L. The magnification was 10,000 ×, while in the inset micrographs, it was 50,000 ×. Images for Ti-Al260, SS-AL180, Ti-HF180 and Ti-HF260 are given in the Supplemental information.

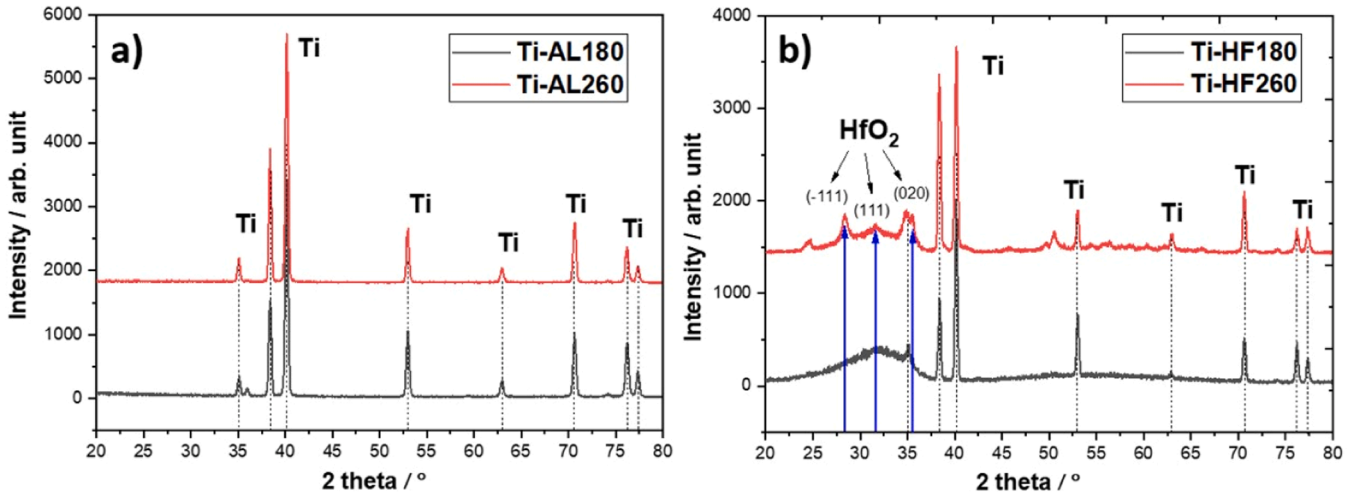

Fig. 2. GI-XRD spectra of **a)** alumina films deposited at 180 °C and 260 °C, and **b)** hafnia films deposited at 180 °C and 260 °C on the cp-Ti substrate.

an amorphous structure as long as ALD deposition is performed below 600 °C [32]. Only peaks for Ti were detected, as these films were too thin to avoid the signal from the substrate.

In contrast to alumina, hafnia films showed different crystallinity at different deposition temperatures. At 180 °C, the XRD spectrum exhibited a broad feature in the range from 25 ° to 40 °C of 2Θ values where peaks for crystalline hafnia are expected (Fig. 2**b**). This feature indicates rather the amorphous structure of the film, possibly with the presence of very small crystallites [37]. TEM analysis showed that nano-sized crystallites or grains were indeed present in the film (Fig. 3**a and b**). The images clearly show the crystallite with a conical shape on the film's surface. After the deposition at 260 °C, hafnia showed a considerably higher proportion of crystallinity (Fig. 2**b**). Reflections for (−111), (111) and (020) crystal planes were observed, which is consistent with the previous investigations [50,56]. TEM analysis of this film showed that all large aggregates, as well as those on the nanometer

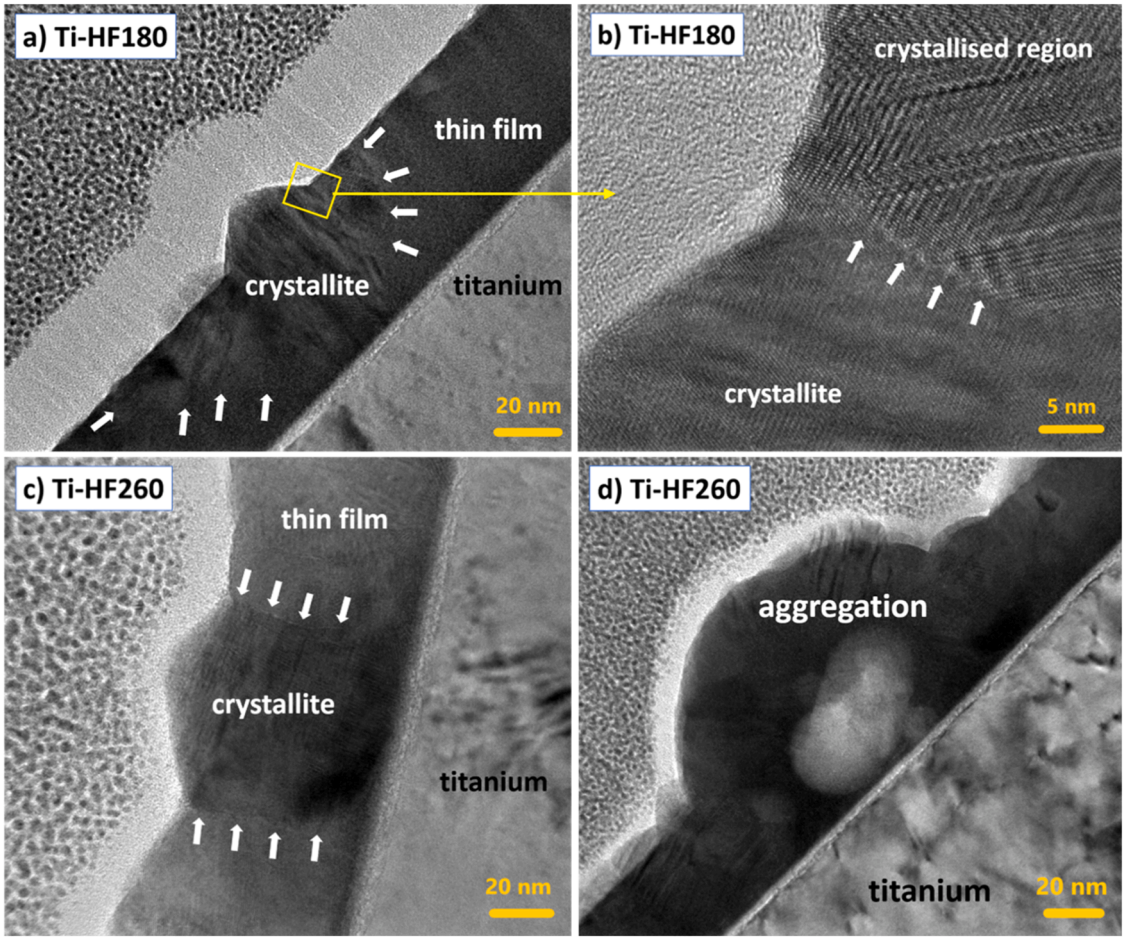

Fig. 3. TEM images of the lamellae prepared by FIB; cross-sections show crystallites of **a, b)** hafnia deposited on cp-Ti at 180 °C and **c, d)** hafnia deposited on cp-Ti at 260 °C. Image (b) presents the area marked by the yellow box in (a) at a larger magnification. The white arrows denote the crystallite boundary.

scale (Fig. 1**d**), were due to the formation of the crystalline phase at 260 °C. An example of a large aggregate is shown in Fig. 3**d**, and a grain is shown in Fig. 3**c**.

Morphologies of alumina and hafnia films (Fig. 1) and TEM images of hafnia on the cross-section sites (Fig. 3) can be used to postulate the modes of films' growth. Generally, there are four growth modes of ALD films: two-dimensional growth mode (layer-by-layer growth or Frank–van der Merwe growth), island growth mode (Volmer–Weber growth), mixed growth mode (Stranski–Krastanov growth) and random deposition or statistical growth mode [40]. Considering the morphology of hafnia films with nanometric grains, island growth mode occurs during the deposition at both temperatures (**insets in** Figs. 1**c and d**), as reported in detail previously [59]. However, when deposited at 260 °C, these grains are much more densely distributed, i.e., the island growth mode is more pronounced at higher temperatures.

For alumina films (Fig. 1**a and b**), surface morphology appears predominantly smooth, and if those large agglomerates are attributed to surface features and defects, it can be concluded that the two-dimensional growth mode prevails. Also, it is consistent with previous reports for ALD alumina films obtained by TMA and water [40].

Regarding the crystallite formation itself, according to the literature, there are three models: 1) growth of a crystallite from initial nuclei embedded in an amorphous film; 2) growth of a crystallite from initial nuclei embedded in an amorphous film, and crystallisation of the amorphous regions next to the grains; 3) growth of ALD film directly in crystalline form, starting from separate crystalline nuclei [32]. In the case of Ti-HF180, it is about the second model, where the initially amorphous region surrounding the crystal grain gradually crystallises during growth (Fig. 3**a and b**), as also reported for TiO_2 [60]. Fig. 3**b** shows the boundary of the crystallite and the surrounding crystallised region. Interestingly, it turned out that this way of growing the film positively affects the film's barrier properties. Namely, electrochemical tests showed this film has excellent impermeability (vide infra).

In the case of Ti-HF260, small crystal grains grow from the substrate with a defined boundary with the surrounding film or other crystallites (Fig. 3**c**). This appearance seems consistent with the third model, which was postulated based on simulation studies [32,61,62]. This way of direct and independent crystallite formation negatively affects the barrier properties of the hafnia film, as shown by electrochemical tests (vide infra). In addition, Ti-HF260 showed large aggregates (Fig. 3**d**), the cause of which is unknown and which exceed the thickness of the film itself. When the crystallites are very large, a model is assumed to be one in which the crystallisation of the amorphous region around the initial grain continues pre-intensively [50,60]. It would mean that the amorphous phase in the hafnia film deposited at 260 °C crystallises enormously around some grains, forming large aggregates. Another possibility is that due to the high deposition temperature (260 °C), which is close to the decomposition temperature of the used precursor (TEMAHf) at around 275 °C [56,63], the adsorbed precursor has been decomposed on some sites on the surface, which is the reason for non-uniformity of the films, and formation of such aggregates.

3.2. *Short-term protective properties*

Fig. 4 shows PDP curves for uncoated cp-Ti and coated specimens with alumina and hafnia films. Cp-Ti is a metal of good corrosion resistance due to passivation in simulated human body conditions. After the Tafel region of the PDP curve, a broad passivation plateau with almost constant current density is established due to the insulating passive film [5,6]. At potentials above 3 V, the current density increases slightly due to the evolution of oxygen, but as valve metal, cp-Ti does not dissolve even at such high potentials [64]. In the previous study, the behaviour of cp-Ti in the same testing conditions was explained in more detail [45].

Regarding the ALD protection, both alumina films reduced the current density by more than two orders of magnitude with a slight increase

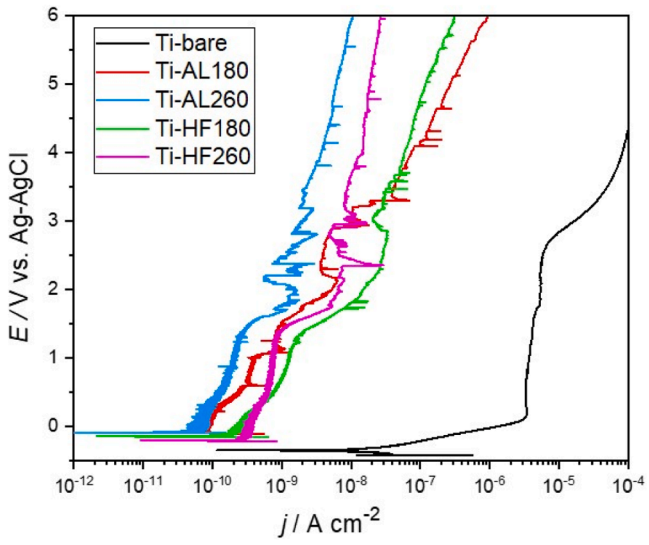

Fig. 4. Potentiodynamic polarisation curves recorded in the Hanks' simulated physiological solution at 37 °C for bare cp-Ti and cp-Ti coated with alumina and hafnia films deposited at 180 °C and 260 °C. $dE/dt = 1$ mV s^{-1}.

in the corrosion potential (Fig. 4). With a further increase in potential, both alumina films, along with the ability of Ti to be passivated, significantly prevent the increase in current. Therefore, alumina films are chemically inert under the tested conditions and have very low porosity. In addition, it can be noticed that the alumina deposited at the higher temperature, Ti-AL260, better retains the increase in current in a broad potential region than alumina deposited at the lower temperature, Ti-AL180. From this, alumina deposited at a higher temperature has slightly better insulating properties than that at a lower temperature, at least from PDP short-term measurements.

In the case of hafnia, a reduction in the corrosion current density is also observed, but slightly less than in the case of the alumina films, which is the consequence of the smaller thickness of the hafnia films (**Figs. S2 and S3**). This reduction is about two orders of magnitude (Fig. 4). A similar behaviour was noticed as for alumina films, i.e. with the increase of the potential in the anodic curve, the current increases faster for the film deposited at a lower temperature, Ti-HF180. This may indicate that the ALD films from alumina and hafnia deposited at a higher temperature have better insulating properties. Considering slightly different thicknesses and comparing the reduction of corrosion current densities of alumina and hafnia films, both seem to offer equal corrosion protection on cp-Ti as the substrate material.

The protective effect of ALD films on the metal surface is even more pronounced on SS316L specimens. Fig. 5 shows the PDP curve of the uncoated SS316L specimen compared to the ALD-coated specimens. SS316L is also known as a metal with good resistance to corrosion in simulated human body conditions [2,6] owing to the formation of the insulating passive film with an outer layer rich in Fe oxide and an inner layer rich in Cr oxide [65,66]. Due to the formation of the oxide layer with a duplex structure, the passive region is established between 0.3 V and 0.6 V with an almost constant current density. Around 0.6 V, the passive film breaks down, and pitting corrosion occurs.

As for cp-Ti, ALD films improve resistance to pitting corrosion and significantly reduce the current density (Fig. 5). Alumina films reduce the corrosion current densities by more than two orders of magnitude. The OCP shifted by 0.25 V more positively, suggesting that the films slowed the anodic reaction compared to bare SS316L. But, what is more significant is that alumina films raised the breakdown potential or the onset of pitting corrosion from 0.6 V for uncoated SS316L to about 1.2 V. Furthermore, similar to the cp-Ti specimens, a slight difference in current density retention is noticeable between alumina deposited at 180 °C and 260 °C. Namely, it seems that alumina deposited at the higher

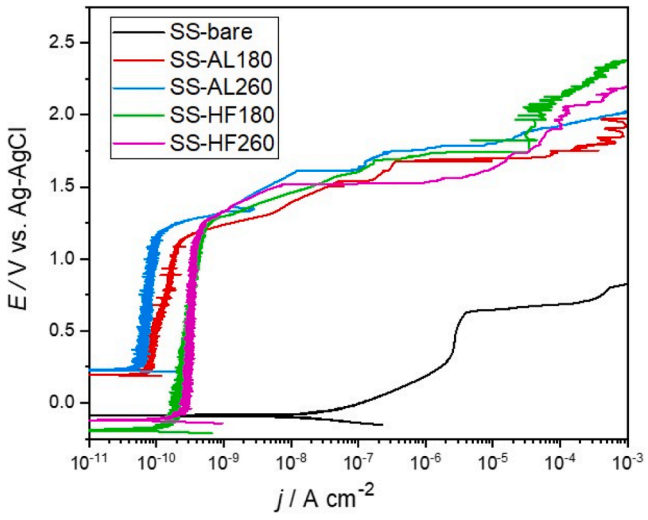

Fig. 5. Potentiodynamic polarisation curves recorded in the Hanks' simulated physiological solution at 37 °C for bare SS316L and SS316L coated with alumina and hafnia films deposited at 180 °C and 260 °C. $dE/dt = 1$ mV s^{-1}.

temperature, SS-AL260, shows better insulating properties because the current density increases somewhat more slowly with the increase in potential than SS-AL180.

The behaviour of the hafnia films on the SS316L is similar to that on the cp-Ti specimens, with a smaller current density reduction than the alumina films due to the smaller thickness of the hafnia (**Figs. S2 and 3**). At the same time, the OCP was more or less unchanged (Fig. 5). Hafnia also raised the breakdown potential to about 1.2 V. However, the difference between hafnia films deposited at different temperatures is not noticeable. More about the efficient protection of alumina and hafnia films on both substrates will be demonstrated from EIS long-term measurements.

3.3. *Long-term protective properties*

Fig. 6 shows the EIS measurements of uncoated cp-Ti and SS316L specimens during 50 days of immersion in the Hanks' simulated physiological solution. Their tendency to be passivated in SBF solutions is observable here as the expansion of the phase angle plateau and its value approaching −90°. The impedance value of cp-Ti increased at low frequencies with immersion time (Fig. 6**a**), resulting from the passive film's increased capacitance due to its thickening [4]. In the case of SS316L, constant impedance values are observed during the immersion period (Fig. 6**b**). However, the insulating properties of the passive film improved, which is evident from the expansion of the plateau of the phase angle curve.

After the deposition of alumina films on cp-Ti and SS316L specimens and EIS testing during 50 days of immersion, significant changes in the electrochemical properties of the specimens are observed (Fig. 7). In the first 30 days, the alumina films Ti-AL180 and Ti-AL260 were stable (Fig. 7**a and b**). The impedance value at low frequencies increased by two orders of magnitude, and the plateau of the phase angle values expanded to almost −90° compared to the uncoated cp-Ti specimen (Fig. 6**a**). This is characteristic of a capacitive surface [67]. Similarly, for the SS-AL180 and SS-AL260 specimens (Fig. 7**c and d**), the increase in impedance values and the expansion of the plateau of the phase angle curve occurred during 30 days of immersion, compared to the uncoated specimen SS316L (Fig. 6**b**). However, for all four types of films (Ti-AL180, Ti-AL260, SS-AL180 and SS-AL260), a narrowing of the phase angle curve and a significant drop in the impedance values can be observed after 40 days of immersion. This coincides with the uncoated specimens after 50 days of immersion (Fig. 6) and indicates a significant instability of alumina during 50 days of EIS testing in the Hanks' solution. The dissolution of alumina films deposited at both temperatures, 180 and 260 °C, was also visually observable due to the loss of the original bluish colour of the films.

Parallel to immersion with EIS testing, one group of specimens was immersed under the same conditions without performing EIS tests. XPS analyses of these differently treated specimens showed unexpected mismatches. Namely, the XPS depth profiles were measured for alumina-coated SS316L specimens that were EIS-tested and that only immersed and not subjected to EIS (Fig. 8). EIS-tested specimens showed the complete absence of alumina on the surface regardless of the deposition temperature (Fig. 8**a and c**), as already observed from the EIS data (Fig. 7**c and d**) and visual inspection of the specimens' surfaces. The presence of Cr oxide in the outer part of the surface layer provides good passivation of the SS316L [68] and is responsible for the high protectiveness of the surface even after the dissolution of the alumina films (Fig. 7**c and d**). However, the specimens immersed for 50 days but not EIS-tested were still covered by the alumina films (Fig. 8**b and d**). For SS-AL180, the thickness of the remaining film was about 10 nm (Fig. 8**b**), while it was not changed for the SS-AL260 (Fig. 8**d**), and it kept the original thickness. In other words, the alumina film, when deposited at a higher temperature (260 °C), remained stable under experimental conditions only if the EIS testing was not performed. Therefore, although applying a very low voltage amplitude of 10 mV (rms) around OCP, the EIS tests have a destructive effect on alumina

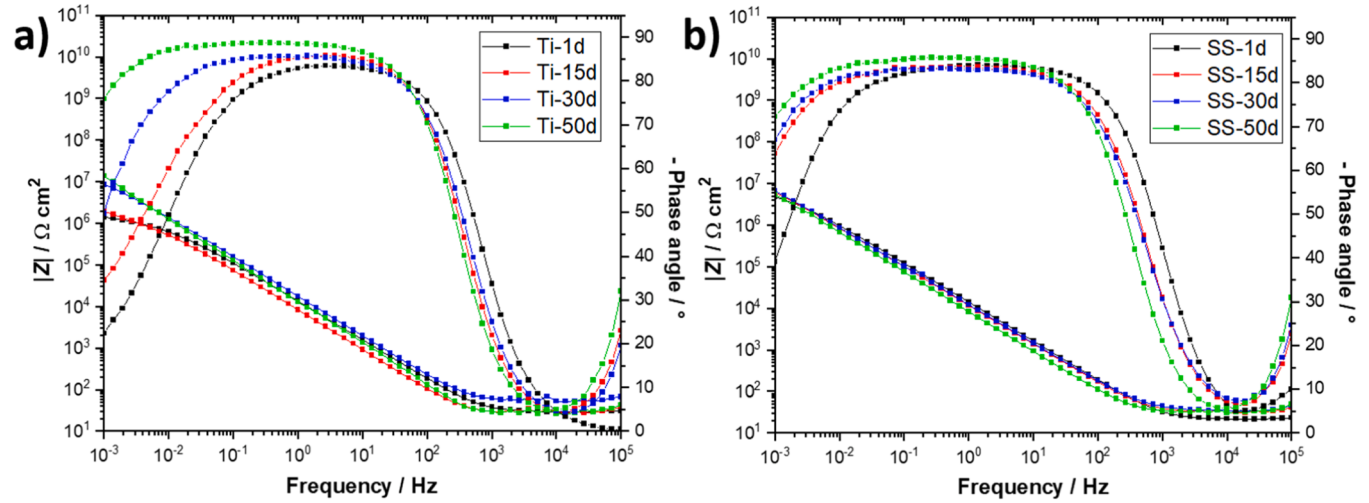

Fig. 6. EIS Bode plots of **a)** uncoated cp-Ti and **b)** SS316L specimens, recorded over 50 days of immersion in the Hanks' simulated physiological solution at 37 °C.

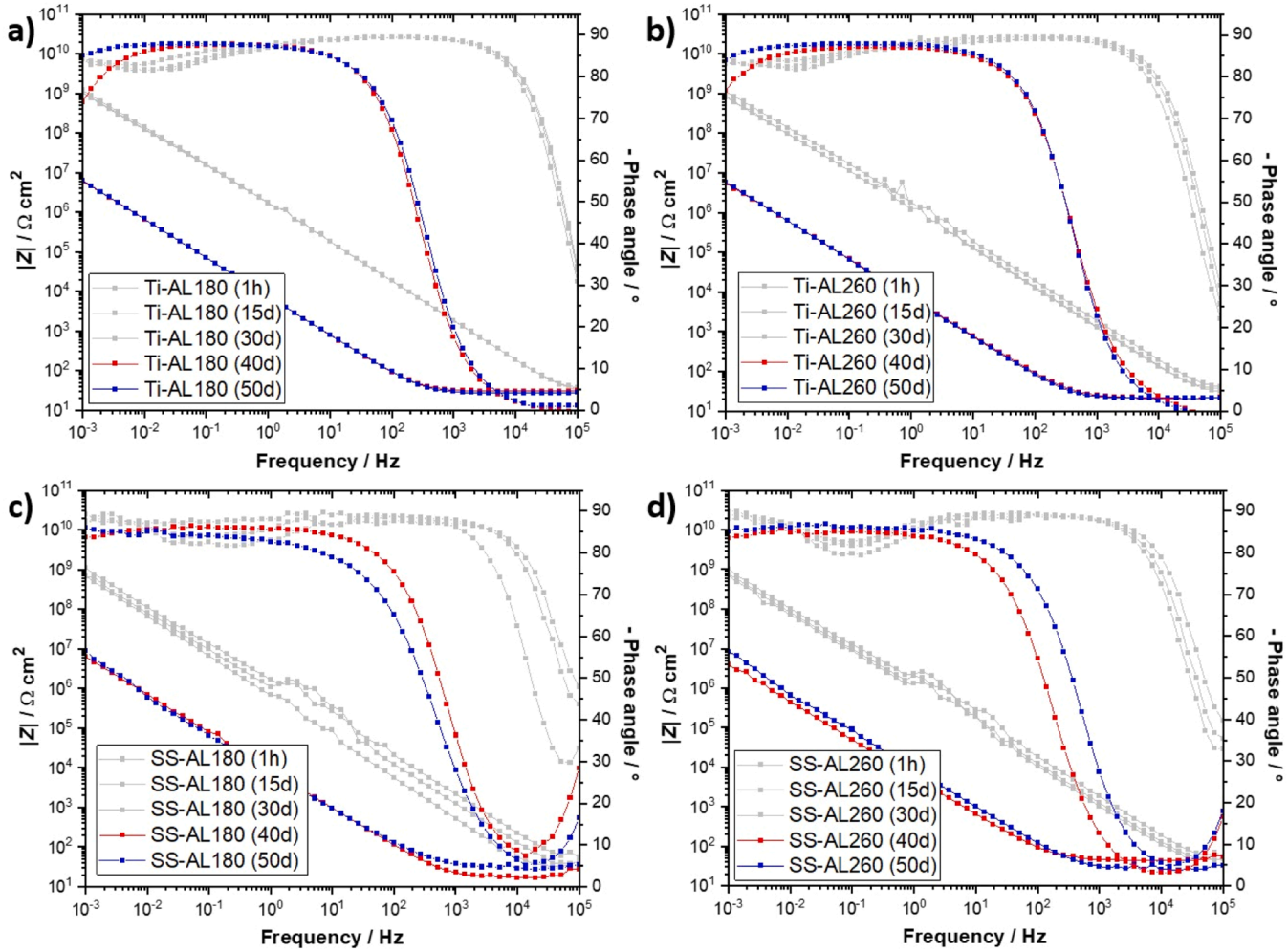

Fig. 7. EIS Bode plots recorded over 50 days of immersion in the Hanks' simulated physiological solution at 37 °C for **a)** cp-Ti coated with alumina deposited at 180 °C, **b)** cp-Ti coated with alumina deposited at 260 °C, **c)** SS316L coated with alumina deposited at 180 °C and **d)** SS316L coated with alumina deposited at 260 °C.

deposited by ALD. Further, it is noteworthy that some previous studies have indicated the possibility of dissolution and instability of alumina deposits, even under very mild conditions [33,34]. So, it is good to emphasize that ALD alumina is almost always amorphous (if subsequent annealing is not carried out [68]) and usually contains a certain proportion of residual hydroxide, i.e. it is not the stoichiometric oxide [32].

Hafnia films showed more promising results of protection in simulated human body conditions. Fig. 9**a and c** show the results of EIS testing of hafnia films deposited at 180 °C on cp-Ti and SS316L specimens. In both cases, excellent stability of the hafnia is maintained during the 50 days of immersion, as the EIS response is unchanged. Impedance values remained high throughout the testing period, and the broad plateau of the phase angle curve almost reached −90°. In the low-frequency region, a slight fall and rise in the value of the phase angle can be seen, which may be related to a low diffusion of the electrolyte in the hafnia film [69]. When deposited at 260 °C (Fig. 9**b and d**), hafnia films did not provide barrier properties during comparatively long immersion times, as did previous specimens. EIS results for Ti-HF260 show that in the first 10 days, the hafnia film provides good protection, i.e. high impedance values and the broad plateau of phase angle values (Fig. 9**b**). However, after 20 days of immersion, the values of the phase angle dropped and after 30 days, even more, indicating the increased porosity of the coating and the exposure of the cp-Ti substrate to the electrolyte. Considering that the impedance value does not decrease totally as in the case of alumina (Fig. 7) but only at low frequencies, it can be concluded that hafnia is stable under these conditions, but its porosity significantly increases over time. Fig. 9**d** shows similar EIS results on the SS316L as substrate. Thus, for a certain period after immersion, the specimen ensures protection, but after 10 days, its barrier properties weaken due to increased porosity, even though the hafnia is inherently stable under these conditions.

The weak barrier properties of the hafnia films deposited at 260 °C can be directly related to the presence of a crystalline phase, which causes high porosity due to the way crystal grains were grown in the film. As shown by the TEM analysis on the Ti-HF260 specimen (Fig. 3**c and d**), grains grown directly on the substrate form a sharp boundary with other grains or with a surrounding amorphous phase, allowing leakage of the electrolyte to the substrate surface. The same was proposed in the case of ALD titania (TiO_2) film, which is prone to crystallisation [20,35]. However, hafnia deposited at 180 °C was very chemically stable, and the crystalline phase was formed gradually during the deposition around the crystal grains and without sharp grain boundaries, creating a non-leakage barrier for the electrolyte (Fig. 9**a and c**). In addition, hafnia deposited at 180 °C also did not contain large aggregates like the one deposited at 260 °C, which likely also affects its barrier properties. Whatever caused the formation of these aggregates (Fig. 3**d**), whether it is intense crystallisation around hafnia grains or precursor decomposition at 260 °C, it can be expected to affect the film's uniformity and its barrier properties.

XPS analyses were performed only for the SS316L samples, and the same result is assumed for the cp-Ti samples due to almost the same EIS results for the SS316L and cp-Ti samples (Fig. 9). Depth profiles show that both hafnia films retain more or less their original thickness of about 60 nm, i.e. they are chemically stable during EIS measurements

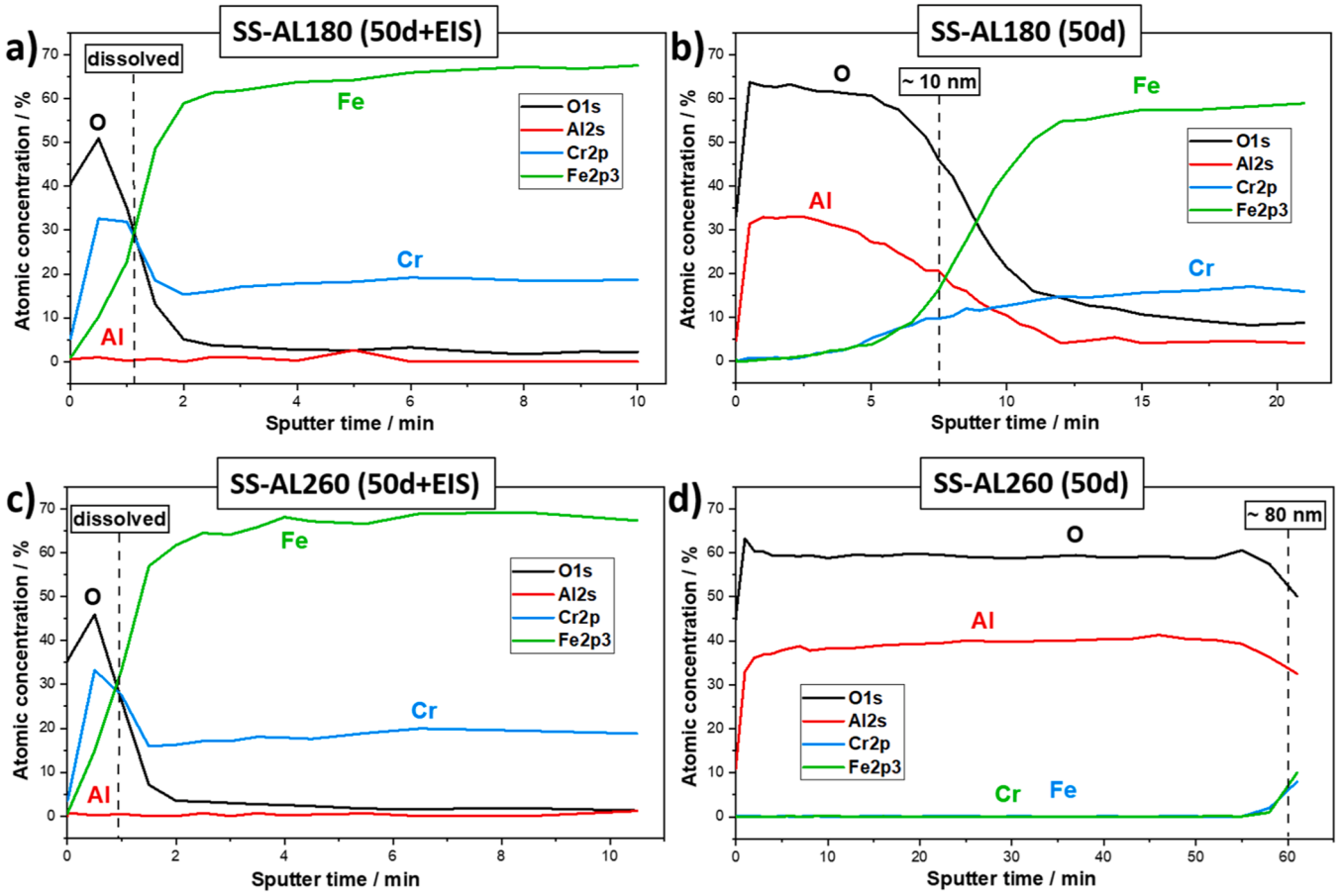

Fig. 8. XPS depth profiles of alumina-coated SS316L specimens after 50 days of immersion in the Hanks' solution at 37 °C with EIS and without EIS testing; **a)** alumina deposited at 180 °C, immersion + EIS testing, **b)** alumina deposited at 180 °C, only immersion, **c)** alumina deposited at 260 °C, immersion + EIS testing and **d)** alumina deposited at 260 °C, only immersion.

(Fig. 10**a and b**). However, on the surface, the situation is a bit more complicated. Namely, surface XPS analyses show a difference between the specimens only immersed and those EIS-tested during the immersion period. Fig. 11 shows the XPS O 1 s spectra for the as-deposited hafnia-coated specimens, those immersed in the Hanks' solution for 50 days, and those immersed and EIS-tested for 50 days. The as-deposited specimens show O 1 s spectrum fitted with the next three component peaks: the first at 530.1 eV corresponding to the oxide (Hf–O), the second at 531.7 eV corresponding to the hydroxide (Hf–OH), and the third at 532.5 eV for adsorbed or coordinated water (HfO_2–HOH) (Fig. 11**a and b**), as previously reported [70,71]. These three peaks appear similar for both hafnia thin films deposited at 180 °C and 260 °C, with the oxide component predominating in both cases. The presence of hydroxide is common in ALD films due to the possibility of incomplete chemical reactions during each deposition cycle [70]. However, the third peak, corresponding to adsorbed or coordinated water, is somewhat unexpected, as it indicates the presence of hydrated species, similar to previous findings [71]. This can be explained by the surface adsorption of water from the cleaning procedure and preparation for characterisation, which leads to surface hydration of the hafnium oxide [72,73].

After 50 days of immersion in Hanks' solution, a significant increase in the proportion of coordinated water can be observed on both hafnia thin film specimens (Fig. 11**c and d**). Therefore, both hafnia thin films significantly adsorb water and undergo the formation of hydrates. The ratio between the two other peaks, i.e., oxide and hydroxide, is significantly altered in favour of the adsorbed water and hydroxide, especially in the case of the hafnia film deposited at a lower temperature. This is evidence that this film is chemically less stable than the one deposited at a higher temperature, and that a transformation process from oxide to hydroxide occurs on the surface. However, as shown by the EIS measurements (Fig. 9), the hafnia deposited at a lower temperature provides excellent barrier properties and maintains its original thickness during 50 days of immersion, as seen from the XPS depth profile. Therefore, it can be concluded that hydroxylation and hydration are surface-limited processes and do not affect the stability of the films in terms of their barrier properties.

After 50 days of EIS testing, the contribution of coordinated water is not as pronounced as in the case of the specimens that were only immersed (Fig. 11**e and f**), i.e., the EIS measurement prevents intensive hydration. Furthermore, it is interesting to observe how successive oxidation and reduction (± 10 mV) at different frequencies during EIS testing affect the surface chemistry of the hafnia thin films deposited at a lower temperature (Fig. 11**e**). The peak at 530.1 eV, corresponding to the oxide, is more prominent compared to the peak at 531.7 eV, corresponding to the hydroxide, unlike the specimen that was only immersed and without the application of EIS measurement (Fig. 11**c**). This indicates that the EIS measurement allows the preservation of the original chemical state of the surface, i.e., the ratio of oxide to hydroxide, through mild oxidation and reduction on the surface. Considering the coordinated water, it can be concluded that the EIS technique induces a competition between oxide and hydroxide species on the surface, accompanied by surface hydration. However, in this study, we did not investigate in detail the surface chemistry of the thin films after EIS measurements, but the results point to the conclusion that the EIS technique contributes to the degradation of alumina and modifies the surface of hafnia thin films, although EIS is commonly regarded as a non-destructive technique.

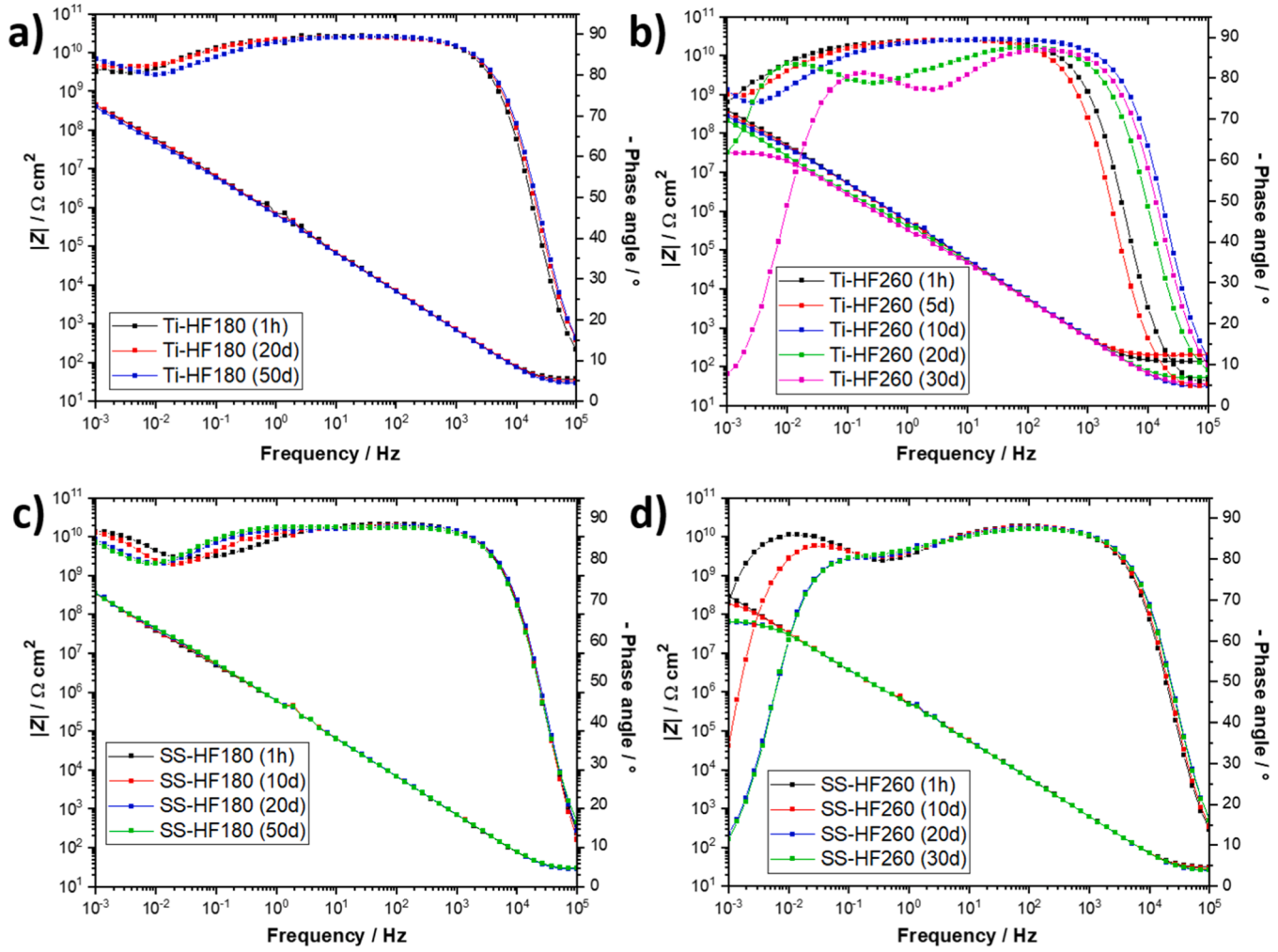

Fig. 9. Bode plots recorded over 50 days of immersion in the Hanks' simulated physiological solution at 37 °C for **a)** cp-Ti coated with hafnia deposited at 180 °C, **b)** cp-Ti coated with hafnia deposited at 260 °C, **c)** SS316L coated with hafnia deposited at 180 °C and **d)** SS316L coated with hafnia deposited at 260 °C.

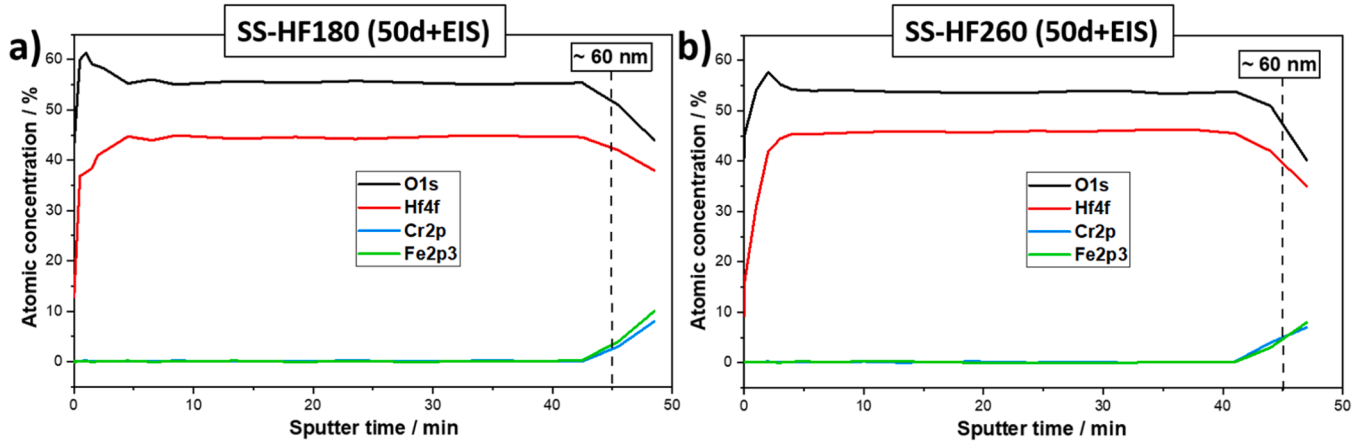

Fig. 10. XPS depth profiles of hafnia-coated SS316L specimens after 50 days of immersion in Hanks' simulated physiological solution at 37 °C with EIS testing; **a)** hafnia deposited at 180 °C and **b)** hafnia deposited at 260 °C.

4. Conclusions

In summary, ALD films of alumina and hafnia deposited on cp-Ti and SS316L substrates significantly reduced corrosion current density in Hanks' simulated physiological solution at 37 °C, thanks to their barrier properties. However, during long-term EIS tests of 50 days, alumina films were chemically unstable and dissolved after 30 days. It was also observed that the EIS technique destructively affects the stability of alumina, regardless of whether deposited at 180 °C or 260 °C, as evidenced by XPS in-depth analysis. It is assumed that successive and slight

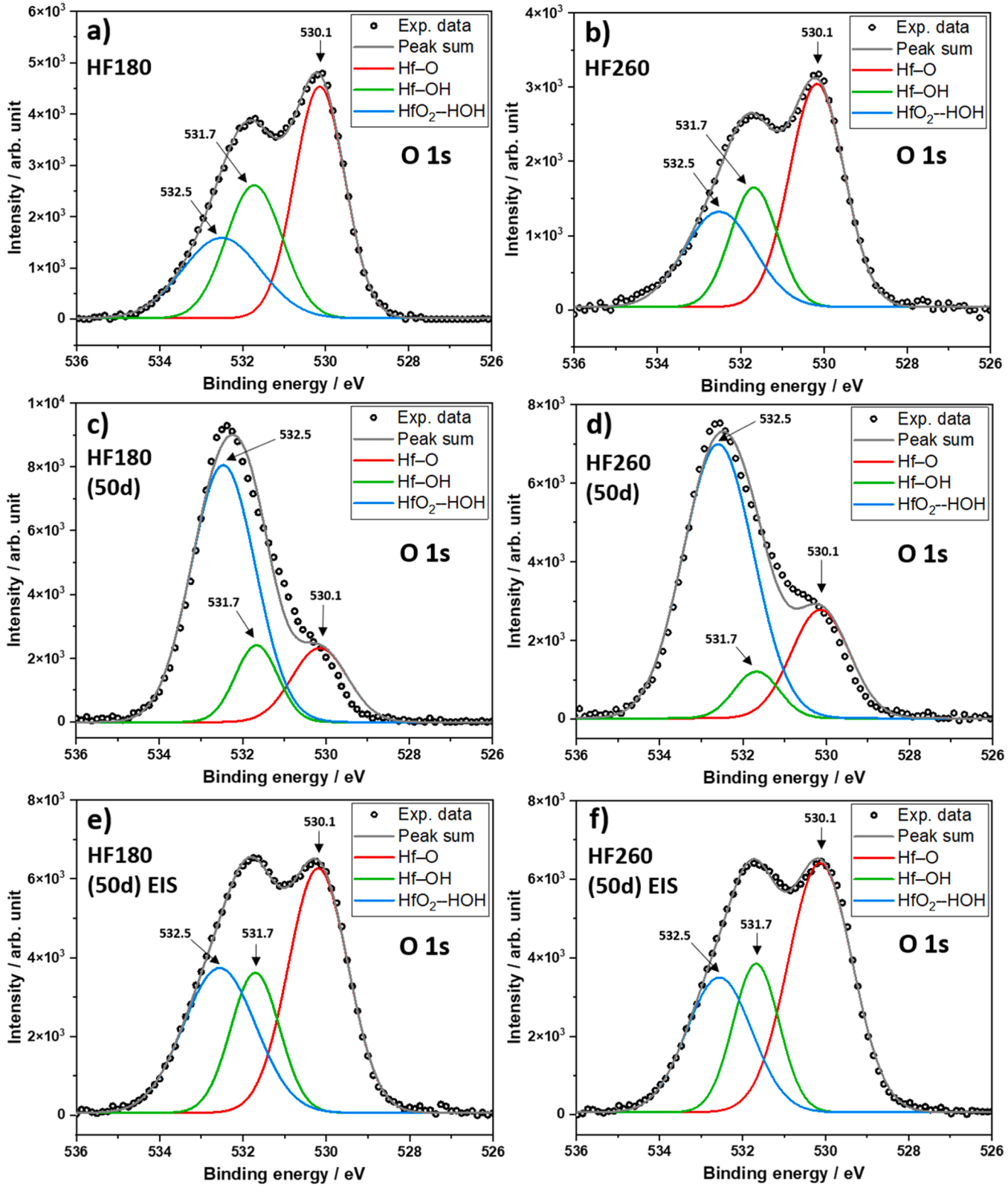

Fig. 11. Experimental and curve-fitted XPS O 1 s spectra of **a)** SS-HF180, **b)** SS-HF260, **c)** SS-HF180 after immersion for 50 days, **d)** SS-HF260 after immersion for 50 days, **e)** SS-HF180 after immersion for 50 days + EIS testing, and **f)** SS-HF260 after immersion for 50 days + EIS testing.

oxidation and reduction applied on the surface of specimens accelerate the hydration of aluminium and turn it into soluble aluminium hydroxide. On the other hand, hafnia films, regardless of the deposition temperature, showed chemical stability during the immersion period, which is evident from XPS depth analyses and EIS testing. Yet, hafnia films deposited at 260 °C have a significantly higher proportion of the crystalline phase, which causes a higher porosity of the film. EIS measurements showed that despite its chemical stability, hafnia deposited at 260 °C does not offer good barrier properties due to the porosity that comes to the fore after a few days of immersion. However, when

deposited at 180 °C, the hafnia films have minimal porosity. This was observed on both substrates, cp-Ti and SS316L. The key difference between hafnia deposited at 180 °C and 260 °C is the proportion and way of formation of crystal grains in these films. The way they are grown at a certain temperature during deposition determines whether the hafnia film will be impermeable or porous after several days of immersion in the tested conditions. XPS analysis also showed that the EIS technique does not act destructively on hafnia as it does on alumina thin films, but rather modifies its surface by partially preventing hydration and controlling the oxide-to-hydroxide ratio on the surface.

CRediT authorship contribution statement

Ivan Spajić: Writing – original draft, Methodology, Investigation, Formal analysis, Data curation, Conceptualization. **Sandra Drev:** Writing – review & editing, Methodology, Formal analysis. **Urška Trstenjak:** Writing – review & editing, Methodology, Funding acquisition. **Ingrid Milošev:** Writing – review & editing, Validation, Supervision, Project administration, Methodology, Conceptualization.

Declaration of competing interest

The authors declare that they have no known competing financial interests or personal relationships that could have appeared to influence the work reported in this paper.

Acknowledgments

This project has received funding from the European Union's Horizon H2020 research and innovation programme under the Marie Skłodowska Curie grant agreement No 764977. Financial support from the Slovenian Research and Innovation Agency (research core funding Nos. P2–0393, IO-0005 and P2–0091) is acknowledged.

Access to scientific equipment (ALD, SEM/FIB and TEM) of the Centre of Excellence in Nanoscience and Nanotechnology – Nanocentre, Ljubljana, and Center for Electron Microscopy and Microanalysis of the Jožef Stefan Institute is acknowledged. The authors are grateful to Dr. Matjaž Spreitzer for providing the XRD measurements and to Prof. Janez Kovač for performing XPS analyses.

Supplementary materials

Supplementary material associated with this article can be found, in the online version, at doi:10.1016/j.electacta.2025.146849.

Data availability

Data will be made available on request.

References

[1] I. Milošev, Metallic materials for biomedical applications: laboratory and clinical studies, Pure Appl. Chem 83 (2011) 309–324, https://doi.org/10.1351/PAC-CON-10-07-09.
[2] N. Eliaz, Corrosion of metallic biomaterials: a review, Materials (Basel) 12 (2019) 1, https://doi.org/10.3390/ma12030407.
[3] K. Prasad, O. Bazaka, M. Chua, M. Rochford, L. Fedrick, J. Spoor, R. Symes, M. Tieppo, C. Collins, A. Cao, D. Markwell, K. Ostrikov, K. Bazaka, Metallic biomaterials: current challenges and opportunities, Materials (Basel) (2017) 10, https://doi.org/10.3390/ma10080884.
[4] J. Pan, D. Thierry, C. Leygraf, Electrochemical and XPS studies of titanium for biomaterial applications with respect to the effect of hydrogen peroxide, J. Biomed. Mater. Res. 28 (1994) 113–122, https://doi.org/10.1002/jbm.820280115.
[5] J. Pan, D. Thierry, C. Leygraf, Electrochemical impedance spectroscopy study of the passive oxide film on titanium for implant application, Electrochim. Acta. 41 (1996) 1143–1153, https://doi.org/10.1016/0013-4686(95)00465-3.
[6] I. Gurappa, Characterization of different materials for corrosion resistance under simulated body fluid conditions, Mater. Charact. 49 (2002) 73–79, https://doi.org/10.1016/S1044-5803(02)00320-0.
[7] M. Niinomi, Mechanical properties of biomedical titanium alloys, Mat. Sci. Eng. A. 243 (1998) 231–236. https://doi.org/10.1016/S0921-5093(97)00806-X.
[8] M. Geetha, A.K. Singh, R. Asokamani, A.K. Gogia, Ti based biomaterials, the ultimate choice for orthopaedic implants - A review, Prog. Mater. Sci. 54 (2009) 397–425, https://doi.org/10.1016/j.pmatsci.2008.06.004.
[9] M.A. Hussein, A.S. Mohammed, N. Al-Aqeeli, Wear characteristics of metallic biomaterials: a review, Materials (Basel) 8 (2015) 2749–2768, https://doi.org/10.3390/ma8052749.
[10] G.D. Rushing, M.J. Goretsky, T. Gustin, M. Morales, R.E. Kelly, D. Nuss, When it is not an infection: metal allergy after the Nuss procedure for repair of pectus excavatum, J. Pediatr. Surg. 42 (2007) 93–97, https://doi.org/10.1016/j.jpedsurg.2006.09.056.
[11] R.I.M. Asri, W.S.W. Harun, M. Samykano, N.A.C. Lah, S.A.C. Ghani, F. Tarlochan, M.R. Raza, Corrosion and surface modification on biocompatible metals: a review, Mat. Sci. Eng. C. 77 (2017) 1261–1274, https://doi.org/10.1016/j.msec.2017.04.102.
[12] P. Budzynski, Long-range effect in nitrogen ion-implanted AISI 316L stainless steel, Nucl. Instrum. Methods Phys. Res. B. 342 (2015) 1–6, https://doi.org/10.1016/j.nimb.2014.09.004.
[13] T.R. Rautray, R. Narayanan, K.H. Kim, Ion implantation of titanium based biomaterials, Prog. Mater. Sci. 56 (2011) 1137–1177, https://doi.org/10.1016/j.pmatsci.2011.03.002.
[14] J.Z. Shi, C.Z. Chen, H.J. Yu, S.J. Zhang, Application of magnetron sputtering for producing bioactive ceramic coatings on implant materials, Bull. Mater. Sci. 31 (2008) 877–884, https://doi.org/10.1007/s12034-008-0140-z.
[15] L. Duta, A.C. Popescu, Current status on pulsed laser deposition of coatings from animal-origin calcium phosphate sources, Coatings 9 (2019) 335, https://doi.org/10.3390/coatings9050335.
[16] G. Giavaresi, L. Ambrosio, G.A. Battiston, U. Casellato, R. Gerbasi, M. Finia, N. N. Aldini, L. Martini, L. Rimondini, R. Giardino, Histomorphometric, ultrastructural and microhardness evaluation of the osseointegration of a nanostructured titanium oxide coating by metal-organic chemical vapour deposition: an in vivo study, Biomaterials 25 (2004) 5583–5591, https://doi.org/10.1016/j.biomaterials.2004.01.017.
[17] M. Leskelä, J. Niinistö, M. Ritala, Atomic layer deposition, in: S. Hashmi (Ed.), Comprehensive Materials Processing, 1st ed., Elsevier Ltd., Oxford, 2014, p. 101.
[18] V. Cremers, R.L. Puurunen, J. Dendooven, Conformality in atomic layer deposition: current status overview of analysis and modelling, Appl. Phys. Rev. 6 (2019) 021302, https://doi.org/10.1063/1.5060967.
[19] M. Ritala, M. Leskelä, J.P. Dekker, C. Mutsaers, P.J. Soininen, J. Skarp, Perfectly conformal TiN and Al_2O_3 films deposited by atomic layer deposition, Chem Vap Depos 5 (1999) 7–9, https://doi.org/10.1002/(SICI)1521-3862(199901)5:1%3C7::AID-CVDE7%3E3.0.CO;2-J.
[20] R. Matero, M. Ritala, M. Leskelä, T. Salo, J. Aromaa, O. Forsén, Atomic layer deposited thin films for corrosion protection, J. Phys. IV. 9 (1999) 493–499, https://doi.org/10.1051/jp4:1999862.
[21] H.C.M. Knoops, S.E. Potts, A.A. Bol, W.M.M. Kessels, Atomic layer deposition, in: Handbook of Crystal Growth: Thin Films and Epitaxy, 2nd Edition, 3, 2015, pp. 1101–1134, https://doi.org/10.1016/B978-0-444-63304-0.00027-5.
[22] M.K. Abbass, S.A. Ajeel, H.M. Wadullah, Biocompatibility, bioactivity and corrosion resistance of stainless steel 316L nanocoated with TiO_2 and Al_2O_3 by atomic layer deposition method, J. Phys. Conf. Ser. 1032 (2018) 012017, https://doi.org/10.1088/1742-6596/1032/1/012017.
[23] F. Wang, Y. Zhang, X. Chen, B. Leng, X. Guo, T. Zhang, ALD mediated heparin grafting on nitinol for self-expanded carotid stents, Colloids Surf. B. 143 (2016) 390–398, https://doi.org/10.1016/j.colsurfb.2016.03.063.
[24] D. Vokoun, L. Klimša, A. Vetushka, J. Duchoň, J. Racek, J. Drahokoupil, J. Kopeček, Y.S. Yu, N. Koothan, C.C. Kei, Al_2O_3 and Pt atomic layer deposition for surface modification of NiTi shape memory films, Coatings 10 (2020) 1–14, https://doi.org/10.3390/COATINGS10080746.
[25] D.S. Finch, T. Oreskovic, K. Ramadurai, C.F. Herrmann, S.M. George, R.L. Mahajan, Biocompatibility of atomic layer-deposited alumina thin films, J. Biomed. Mater. Res. A. 87 (2008) 100–106, https://doi.org/10.1002/jbm.a.31732.
[26] Q. Yang, W. Yuan, X. Liu, Y. Zheng, Z. Cui, X. Yang, H. Pan, S. Wu, Atomic layer deposited ZrO_2 nanofilm on Mg-Sr alloy for enhanced corrosion resistance and biocompatibility, Acta. Biomater 58 (2017) 515–526, https://doi.org/10.1016/j.actbio.2017.06.015.
[27] M. Peron, A. Bin Afif, A.L. Dadlani, F. Berto, J. Torgersen, Improving stress corrosion cracking behavior of AZ31 alloy with conformal thin titania and zirconia coatings for biomedical applications, J. Mech. Behav. Biomed. Mater. 111 (2020) 104005, https://doi.org/10.1016/j.jmbbm.2020.104005.
[28] A. Zięboowicz, A. Sambok-Kiełbowicz, W. Walke, A. Mzyk, K. Kosiel, J. Kubacki, B. Bączkowski, M. Pawlyta, B. Zięboowicz, Evaluation of bacterial adhesion to the ZrO_2 atomic layer deposited on the surface of cobalt-chromium dental alloy produced by DMLS method, Materials (Basel) 14 (2021) 1–15, https://doi.org/10.3390/ma14051079.
[29] I.P. Grigal, A.M. Markeev, S.A. Gudkova, A.G. Chernikova, A.S. Mityaev, A. P. Alekhin, Correlation between bioactivity and structural properties of titanium dioxide coatings grown by atomic layer deposition, Appl. Surf. Sci. 258 (2012) 3415–3419, https://doi.org/10.1016/j.apsusc.2011.11.082.
[30] M. Shahmohammadi, B. Yang, C.G. Takoudis, Applications of titania atomic layer deposition in the biomedical field and recent updates, Am. J. Biomed. Sci. Res. 8 (2020) 465–468, https://doi.org/10.34297/ajbsr.2020.08.001321.
[31] M. Putkonen, T. Sajavaara, P. Rahkila, L. Xu, S. Cheng, L. Niinistö, H.J. Whitlow, Atomic layer deposition and characterization of biocompatible hydroxyapatite thin

films, Thin Solid. Films 517 (2009) 5819–5824, https://doi.org/10.1016/j.tsf.2009.03.013.
[32] V. Miikkulainen, M. Leskelä, M. Ritala, R.L. Puurunen, Crystallinity of inorganic films grown by atomic layer deposition: overview and general trends, J. Appl. Phys. 113 (2013) 021301, https://doi.org/10.1063/1.4757907.
[33] G.C. Correa, B. Bao, N.C. Strandwitz, Chemical stability of titania and alumina thin films formed by atomic layer deposition, ACS Appl. Mater. Interfaces. 7 (2015) 14816–14821, https://doi.org/10.1021/acsami.5b03278.
[34] A.I. Abdulagatov, Y. Yan, J.R. Cooper, Y. Zhang, Z.M. Gibbs, A.S. Cavanagh, R. G. Yang, Y.C. Lee, S.M. George, Al_2O_3 and TiO_2 atomic layer deposition on copper for water corrosion resistance, ACS Appl. Mater. Interfaces 3 (2011) 4593–4601, https://doi.org/10.1021/am2009579.
[35] J.S. Daubert, G.T. Hill, H.N. Gotsch, A.P. Gremaud, J.S. Ovental, P.S. Williams, C. J. Oldham, G.N. Parsons, Corrosion protection of copper using Al_2O_3, TiO_2, ZnO, HfO_2, and ZrO_2 atomic layer deposition, ACS Appl. Mater. Interfaces. 9 (2017) 4192–4201, https://doi.org/10.1021/acsami.6b13571.
[36] D.M. Hausmann, E. Kim, J. Becker, R.G. Gordon, Atomic layer deposition of hafnium and zirconium oxides using metal amide precursors, Chem Mater 14 (2002) 4350–4358, https://doi.org/10.1021/cm020357x.
[37] D. Blaschke, F. Munnik, J. Grenzer, L. Rebohle, H. Schmidt, P. Zahn, S. Gemming, A correlation study of layer growth rate, thickness uniformity, stoichiometry, and hydrogen impurity level in HfO_2 thin films grown by ALD between 100°C and 350°C, Appl. Surf. Sci. 506 (2020) 144188, https://doi.org/10.1016/j.apsusc.2019.144188.
[38] A.K. Bishal, A. Butt, S.K. Selvaraj, B. Joshi, S.B. Patel, S. Huang, B. Yang, T. Shukohfar, C. Sukotjo, C.G. Takoudis, Atomic layer deposition in bio-nanotechnology: a brief overview, Crit. Rev. Biomed. Eng. 43 (2015) 255–276, https://doi.org/10.1615/CritRevBiomedEng.2016016456.
[39] S.A. Skoog, J.W. Elam, R.J. Narayan, Atomic layer deposition: medical and biological applications, Int. Mater. Rev. 58 (2013) 113–129, https://doi.org/10.1179/1743280412Y.0000000009.
[40] R.L. Puurunen, Surface chemistry of atomic layer deposition: a case study for the trimethylaluminum/water process, J. Appl. Phys. 97 (2005) 121301, https://doi.org/10.1063/1.1940727.
[41] M. Rahmati, M. Mozafari, Biocompatibility of alumina-based biomaterials–A review, J. Cell Physiol. 234 (2019) 3321–3335, https://doi.org/10.1002/jcp.27292.
[42] H.H. Al-Moameri, Z. Majid Nahi, D. Raheem Rzaij, N.T. Al-Sharify, A review on the biomedical applications of alumina, J. Eng. Sustain. Dev. 24 (2020) 28–36, https://doi.org/10.31272/jeasd.24.5.5.
[43] K. Kukli, J. Aarik, M. Ritala, T. Uustare, T. Sajavaara, J. Lu, J. Sundqvist, A. Aidla, L. Pung, A. Hårsta, M. Leskelä, Effect of selected atomic layer deposition parameters on the structure and dielectric properties of hafnium oxide films, J. Appl. Phys. 96 (2004) 5298–5307, https://doi.org/10.1063/1.1796513.
[44] M.J. Biercuk, D.J. Monsma, C.M. Marcus, J.S. Backer, R.G. Gordon, Low-temperature atomic-layer-deposition lift-off method for microelectronic and nanoelectronic applications, Appl. Phys. Lett. 83 (2003) 2405–2407, https://doi.org/10.1063/1.1612904.
[45] I. Spajić, P. Rodič, G. Šekularac, M. Lekka, L. Fedrizzi, I. Milošev, The effect of surface preparation on the protective properties of Al_2O_3 and HfO_2 thin films deposited on cp-titanium by atomic layer deposition, Electrochim. Acta. 366 (2021) 137431, https://doi.org/10.1016/j.electacta.2020.137431.
[46] Z. Fohlerova, A. Mozalev, Anodic formation and biomedical properties of hafnium-oxide nanofilms, J. Mater. Chem. B. 7 (2019) 2300–2310, https://doi.org/10.1039/c8tb03180k.
[47] H. Matsuno, A. Yokoyama, F. Watari, M. Uo, T. Kawasaki, Biocompatibility and osteogenesis of refractory metal implants, titanium, hafnium, niobium, tantalum and rhenium, Biomaterials 22 (2001) 1253–1262, https://doi.org/10.1016/S0142-9612(00)00275-1.
[48] S. Mohammadi, M. Esposito, M. Cucu, L.E. Ericson, P. Thomsen, Tissue response to hafnium, J. Mater. Sci. Mater. Med. 12 (2001) 603–611, https://doi.org/10.1023/A:1011237610299.
[49] F. Zhang, G. Liu, A. Liu, B. Shin, F. Shan, Solution-processed hafnium oxide dielectric thin films for thin-film transistors applications, Ceram. Int. 41 (2015) 13218–13223, https://doi.org/10.1016/j.ceramint.2015.07.099.
[50] D.M. Hausmann, R.G. Gordon, Surface morphology and crystallinity control in the atomic layer deposition (ALD) of hafnium and zirconium oxide thin films, J. Cryst. Growth. 249 (2003) 251–261, https://doi.org/10.1016/S0022-0248(02)02133-4.
[51] I. Spajić, E. Rahimi, M. Lekka, R. Offoiach, L. Fedrizzi, I. Milošev, Al_2O_3 and HfO_2 atomic layers deposited in single and multilayer configurations on titanium and on stainless steel for biomedical applications, J. Electrochem. Soc. 168 (2021) 071510, https://doi.org/10.1149/1945-7111/ac131b.
[52] I. Spajić, M.G. Morais, C. Monteiro, M.C.L. Martins, A.P. Pego, I. Milošev, Biocompatibility and antibacterial properties of medical stainless steel and titanium modified by alumina and hafnia films prepared by atomic layer deposition, J. Mater. Sci. Mater. Med. 35 (2024) 68, https://doi.org/10.1007/s10856-024-06841-8.
[53] M. Putkonen, M. Nieminen, L. Niinistö, Magnesium aluminate thin films by atomic layer deposition from organometallic precursors and water, Thin Solid Films 466 (2004) 103–107, doi https://doi.org/10.1016/j.tsf.2004.02.078.
[54] R. Matero, A. Rahtu, M. Ritala, M. Leskelä, T. Sajavaara, Effect of water dose on the atomic layer deposition rate of oxide thin films, Thin Solid Films 368 (2000) 1–7, https://doi.org/10.1016/S0040-6090(00)00890-7.
[55] C.H. Chang, Y.K. Chiou, C.W. Hsu, T.B. Wu, Hydrous-plasma treatment of Pt electrodes for atomic layer deposition of ultrathin high- k oxide films, Electrochem. Solid-State Lett. 10 (2007) 5–8, https://doi.org/10.1149/1.2426411.
[56] K. Kukli, M. Ritala, T. Sajavaara, J. Keinonen, M. Leskelä, Atomic layer deposition of hafnium dioxide films from hafnium tetrakis(ethylmethylamide) and water, Chem Vap Depos 8 (2002) 199–204, https://doi.org/10.1002/1521-3862(20020903)8:5 %3C199::AID-CVDE199 %3E3.0.CO;2-U.
[57] T. Nam, S. Seo, H. Kim, Atomic layer deposition of a uniform thin film on two-dimensional transition metal dichalcogenides, J. Vac. Sci. Technol. A. 38 (2020) 030803, https://doi.org/10.1116/6.0000068.
[58] S. McDonnell, B. Brennan, A. Azcatl, N. Lu, H. Dong, C. Buie, J. Kim, C.L. Hinkle, M.J. Kim, R.M. Wallace, HfO_2 on MoS_2 by atomic layer deposition: adsorption mechanisms and thickness scalability, ACS Nano 7 (2013) 10354–10361, https://doi.org/10.1021/nn404775u.
[59] X. Nie, F. Ma, D. Ma, K. Xu, Growth mode evolution of hafnium oxide by atomic layer deposition, J. Vac. Sci. Technol. A. 32 (2014) 01A109, https://doi.org/10.1116/1.4832224.
[60] R.L. Puurunen, T. Sajavaara, E. Santala, V. Miikkulainen, T. Saukkonen, M. Laitinen, M. Leskelä, Controlling the crystallinity and roughness of atomic layer deposited titanium dioxide films, J. Nanosci. Nanotechnol. 11 (2011) 8101–8107, https://doi.org/10.1166/jnn.2011.5060.
[61] O. Nilsen, O.B. Karlsen, A. Kjekshus, H. Fjellvåg, Simulation of growth dynamics in atomic layer deposition. Part II. Polycrystalline films from cubic crystallites, Thin Solid Films 515 (2007) 4538–4549, https://doi.org/10.1016/j.tsf.2006.11.024.
[62] O. Nilsen, O.B. Karlsen, A. Kjekshus, H. Fjellvåg, Simulation of growth dynamics in atomic layer deposition. Part III. Polycrystalline films from tetragonal crystallites, Thin Solid Films 515 (2007) 4550–4558, https://doi.org/10.1016/j.tsf.2006.11.025.
[63] N.K. Oh, J.-T. Kim, J.-K. Ahn, G. Kang, S.Y. Kim, J.-Y. Yun, The effects of thermal decomposition of tetrakis-ethylmethylaminohafnium (TEMAHf) precursors on HfO_2 film growth using atomic layer deposition, Appl. Sci. Converg. Technol. 25 (2016) 56–60, https://doi.org/10.5757/asct.2016.25.3.56.
[64] J.W. Schultze, M.M. Lohrengel, Stability, reactivity and breakdown of passive films. Problems of recent and future research, Electrochim. Acta. 45 (2000) 2499–2513, https://doi.org/10.1016/S0013-4686(00)00347-9.
[65] V. Maurice, P. Marcus, Current developments of nanoscale insight into corrosion protection by passive oxide films, Curr. Opin. Solid. State Mater. Sci. 22 (2018) 156–167, https://doi.org/10.1016/j.cossms.2018.05.004.
[66] I. Milošev, H.H. Strehblow, The behavior of stainless steels in physiological solution containing complexing agent studied by x-ray photoelectron spectroscopy, J. Biomed. Mater. Res. 52 (2000) 404–412, https://doi.org/10.1002/1097-4636(200011)52:2<404::AID−JBM22>3.0.CO;2-Z.
[67] B. Van Der Linden, H. Terryn, J. Vereeckem, Investigation of anodic aluminium oxide layers by electrochemical impedance spectroscopy, J. Appl. Electrochem. 20 (1990) 798–803, https://doi.org/10.1007/BF01094309.
[68] M. Broas, O. Kanninen, V. Vuorinen, M. Tilli, M. Paulastokro-Kröckel, Chemically stable atomic-layer-deposited Al_2O_3 films for processability, ACS Omega 2 (2017) 3390–3398, https://doi.org/10.1021/acsomega.7b00443.
[69] S. Tamilselvi, R. Murugaraj, N. Rajendran, Electrochemical impedance spectroscopic studies of titanium and its alloys in saline medium, Mater. Corr. 58 (2007) 113–120, https://doi.org/10.1002/maco.200603979.
[70] D. Barreca, A. Milanov, R.A. Fischer, A. Devi, E. Tondello, Hafnium oxide thin film grown by ALD: an XPS study, Surf. Sci. Spectra. 14 (2007) 34–40, https://doi.org/10.1116/11.20080401.
[71] X. Yang, F. Zhao, Y.W. Yeh, R.S. Selinsky, Z. Chen, N. Yao, C.G. Tully, Y. Ju, B. E. Koel, Nitrogen-plasma treated hafnium oxyhydroxide as an efficient acid-stable electrocatalyst for hydrogen evolution and oxidation reactions, Nat. Commun. 10 (2019) 1543, https://doi.org/10.1038/s41467-019-09162-5.
[72] I.B. Polovov, Y.S. Bataev, Y.D. Afonin, V.A. Volkovich, A.V. Chukin, A. Rakhmatullin, M. Boča, Synthesis of HfO_2 from hafnium hydroxide hydrate, J. Alloys Compd. 790 (2019) 405–412, https://doi.org/10.1016/j.jallcom.2019.03.103.
[73] S. Hong, S.P. Park, Y. Kim, B.H. Kang, J.W. Na, H.J. Kim, Low-temperature fabrication of an HfO_2 passivation layer for amorphous indium–gallium–zinc oxide thin film transistors using a solution process, Sci. Rep. 7 (2017) 16265, https://doi.org/10.1038/s41598-017-16585-x.